SWhegPro3: A Three-Impeller Wheel-Leg Transformable Robot with Variable Robust Adaptability to Stair Dimensions

Haoran Wang, Siyuan Wang, Cunxi Dai, Zhenzhong Jia*

***Abstract*— This paper reports the design innovation and implementation of a novel wheel-leg transformable robot named SWhegPro3. The robot uses a three-impeller design to significantly improve the overall stair-climbing performance. Unlike other impeller-based designs that use gear sets to unfold the impellers, this robot uses self-locking electric push rods for mode switching, thereby greatly improving its load capacity. We also analyze the stair climbing operation and derive a model to calculate the optimal configuration of the wheel-leg module and the corresponding displacement of the push rod, in order to better adapt to different sized stairs. We conduct both simulation and field experiments to validate our proposed design and control strategy.**

I. Introduction

Mobile stability and operational efficiency are important indicators for evaluating the mobile robot's performance. The indoor ground can be divided into two cases: flat floor and stairs. Wheeled robots are widely used to efficiently transport goods on flat ground, but they are difficult to navigate through uneven surfaces, especially stair and step climbing cases. Legged robots have superior mobility over rugged ground and stairs, but their motion smoothness and operating efficiency under high loads over flat ground fall far behind wheeled robots. This paper aims to develop a robot that can take advantages of both legged and wheeled motion modalities to achieve good overall performance [1].

Agile legged robots are often considered to be the best solution for complex, stair-climbing environments. For example, in recent years, quadruped robots such as Spot-Mini have demonstrated very good capability in climbing up and down stairs quickly and reliably. Although these legged robots imitate animal leg structure and integrate various advantages of animal mobility, their motion mechanism and control strategy in complex scenes are quite complicated. Also, their load capacity are often limited by the output torque of their joint motors. For legged mode, we prefer robots with simple control architecture (e.g., RHex [2]–[4]) to navigate stair obstacles, as well as high payload capacity.

The wheel-leg transformable robot is considered to be a good balance between wheeled and legged modes by taking their respective advantages: speed and operation efficiency over flat ground in wheel mode, obstacle negotiation capability over uneven terrain and stair cases in leg mode. Various schemes have been proposed to achieve this goal. For example, various special wheel structure designs, e.g., Epi.q series robots [5], can use the characteristics of the mechanism to passively adjust their motion state over irregular terrains; they can also drive the wheel set over obstacles such as steps. The Land Devil Ray (LDR) robot [6] can passively trigger its leg structure to open state when encountering obstacles such as stairs through a multi-link mechanism, then apply torque to the contact point between its toes and steps to lift the wheelset. The RHyMo robot [7] utilizes an additional rocker arm - a bogie platform that lifts the body to help cross obstacles such as stairs. Although many wheel-leg robot solutions can achieve both flat ground and stair-climbing mobility scenarios, they do not take into account structural reliability, moving stability, moving speed, and other factors.

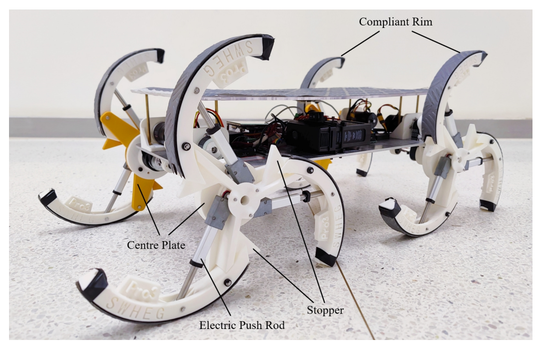

Fig. 1. SWhegPro3: our wheel-leg transformable robot for stair climbing.

Previously, our team has developed a wheel-leg transformable robot named SWhegPro [8] that can operate with high energy efficiency in different ground scenarios. Its unique heterosexual wheel structure allows the robot to traverse the terrain with different gait strategies. It can adjust the wheel mode in different surface situations to obtain better load capacity. It also has certain mobility in short-step and stair-climbing scenarios. However, the switching actuator (push rods) in its wheel-leg module only operates in fully-open (leg mode) and fully-closed (wheel mode) states, limiting its adaptability to step/stair sizes. Also, its wheel-leg module essentially acts as an S-shape structure, whose stair negotiation capability falls far behind three-impeller (see Fig. 1) or curved-spoke mechanism [9].

This paper introduces our newly developed, more stable and robust wheel-leg transformable robot platform: SWhegPro3, as shown in Fig. 1. When operating in leg mode, the wheel-leg module has a similar shape to the fixed curved-spoke tri-wheel mechanism shown in [9]. Moreover, we can adjust its shape by controlling the displacement of the push

All authors are with the Shenzhen Key Laboratory of Biomimetic Robotics and Intelligent Systems, Department of Mechanical and Energy Engineering, Southern University of Science and Technology (SUSTech), Shenzhen, 518055, China. They are also with Guangdong Provincial Key Laboratory of Human-Augmentation and Rehabilitation Robotics in Universities, SUSTech, Shenzhen, 518055, China. *Corresponding author: jiazz@sustech.edu.cn

rod actuator in the wheel-leg module, in order to greatly improve the robot's stability and mobility over different-sized stairs, ensuring its adaptability. In addition, the most vulnerable parts of the spokes are not subject to the greatest torque load during climbing, so lighter composite materials can be used instead of metal spokes to reduce body weight.

The main contributions of this paper are:

- We propose a wheel-leg transformable robot with three-impeller design, which greatly improves its stair climbing capability. The self-locking push rod switching actuator greatly improves the robot load capacity.
- We analyze the stair climbing operation and derive a model to calculate the optimal displacement of the push rod actuator for different sized stairs.
- We conduct both simulation and field experiments to validate our proposed design and control strategy.

II. Robot Hardware Design

A. Modular Design of the Transformable Wheel Mechanism

From our previous experience, the wheel-leg transformable module is influenced by its leg mode design. Inspired by [9] and other literature [10], we find that the curved-spoke mechanism, i.e., the three-impeller structure, holds great promise for stair climbing. However, the robot in [9] adopts a tri-wheel design, with two driven three-impeller wheels and a passive castor or spherical wheel to support the body. This design fails to perform smooth and efficient actions for stair-climbing because it only has two driven wheels. Also, the envelopes of the driven wheels are not round, leading to very poor performance with unacceptable impacts over flat ground. To solve these problems, as shown in Fig. 1, we develop a robot with four wheel-leg modules, each of which incorporates the distinctive curved-spoke three-impeller design (inspired by [9]) for legged mode operation.

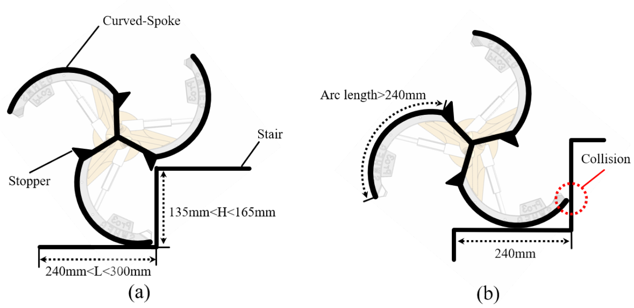

Fig. 2. Design guidance for wheel-leg structure dimensions. (a) The stopper height should exceed the upper stair when the end point of curve-spoke touches the lower stair. (b) The arc-length should not exceed the horizontal length of stairs, otherwise, it will result in unwanted collisions.

Based on the stair standards in China, we reevaluate the geometric parameters for the wheel-leg module. The designated dimensions for our target stairs are $240-300mm$ in length and $135-165mm$ in height. Following the kinematic analysis, we determine that the amplitude of the spoke opening should be determined by the maximum height of typical stairs. The underlying principle is depicted in Fig. 2(a). The arc length of the compliant rim corresponds to the minimum length of typical stairs. This design ensures that the wheel spokes do not collide with the vertical plane of the stairs. The principle is shown in Fig. 2(b). We retain the stopper within the curved-spoke mechanism [9]. This stopper's reset function enhances the robot's fault tolerance during climbing. In the compliant rim depicted in Fig. 3(a), each individual spoke within the three-impeller structure is precisely one-third of the entire wheel. With these in mind, we intend to design a transformable structure that enables the wheel to transform smoothly between the three-impeller configuration and the standard wheel structure.

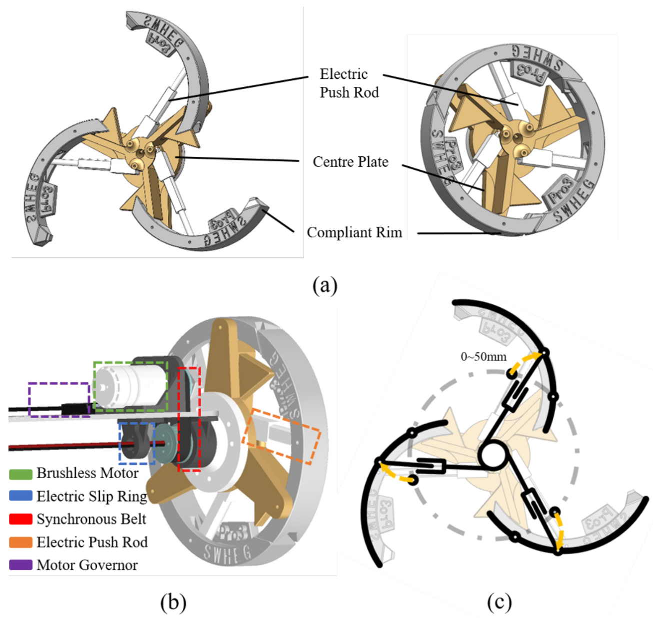

Fig. 3. Mechanical design of transformable wheel-leg structure. (a) The wheel and leg modes. (b) Components of the modular wheel-leg structure. (c) Schematic diagram of the electric push rod during mode switching.

Similar to our SWhegPro robot [8], we use electric push rod actuator for wheel-leg mode switching, as shown in Fig. 3(c). Its self-locking property provides good reliability and payload performance, especially when compared to gear set used in [10]. The signal line and power supply of these electric push rods are connected to the H-bridge controller via a conductive slip ring. The driven wheel involves a timing pulley set in motion by a timing belt, which is itself driven by a motor through another timing pulley. The interconnection of these components is shown in Fig. 3(a) and (b).

B. Determining Proper Wheelbase

We then transit the tri-wheel mechanism to a four-wheel drive robot. As the four-wheel drive configuration introduces an additional pair of drive wheels in contrast to the tri-wheel mechanism, it becomes essential to determine an appropriate linkage between the front and rear wheels.

By using Matlab, we conduct a kinematic analysis of the simplified robot: Initially, there is an ideal wheel trajectory in the stair-climbing process of a single wheel. Then we assume that no slippage between the spokes and the stairs and all wheels will follow the same ideal trajectory to ensure stable motion. Because of the linkage between the front and rear wheels, we can subsequently solve the geometric center trajectory of the robot when we obtain the position sets of the front wheels. The trajectory of the geometric center with a wheelbase of $500mm$ is depicted in Fig. 4(a).

Then we obtain the best wheelbase by using a fitting optimization method: Considering that the geometric center trajectory of the robot should align well with the slope of the staircase, we calculate the root mean square error (RMSE) between the trajectory and the slope line as our evaluation metric. We ultimately select $510mm$ as the optimal wheelbase parameter, leading to the smoothest climbing motion. Figure 4(b) illustrates the fitting root mean square error for wheelbases ranging from $300mm$ to $600mm$ while considering a staircase dimension of $300mm \times 160mm$.

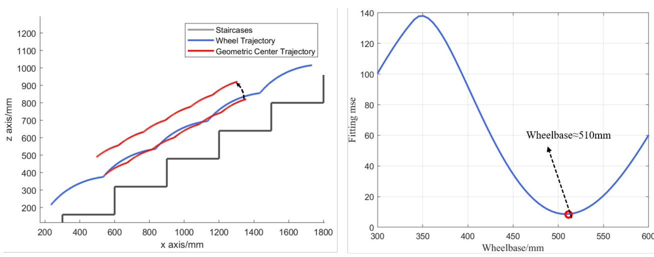

(a) (b)

Fig. 4. Visualization demo for the ideal center trajectory optimization. (a)Wheel trajectory and geometric center trajectory. (b)Optimization of wheelbase by using RMSE method.

III. Mechatronics System Design

The chosen motion control components and data sampling modules align closely with those used in the SWhegPro project. The central computing unit of the robot is the Raspberry Pi 4B embedded computer, and communication between modules is facilitated by the Robot Operating System (ROS). Four DJI M3508 brushless gear motors function as the propulsion units, with each motor being controlled by a DJI C620 FOC controller. CAN signals from the FOC controller are converted to USB signals by a translator. For data acquisition during the robot's movement, the IMU module plays a predominant role. Each modular wheel is independently managed by three electric push rods which are manipulated by PWM signals to extend the wheel spokes. The wheelset itself is fashioned from PLA material through 3D printing. s Shock-absorbing cotton and PVC pads are added to the outer edge of the wheel to dampen impact forces and slippery.

IV. Driving Strategy

A. Two driving strategies

The SWhegPro3 has two distinct driving strategies: (1) Flat ground driving strategy: the vehicle operates as a four-wheel differential-driven vehicle, where the desired speed and yaw angle can be given by the remote control interface. (2) Stair-climbing strategy: When encountering stairs, the electric push rods extend, enabling the robot to climb stairs.

We add a transition state between the wheeled state and the legged state to reset the phase between the left and right wheels, which can ensure the symmetry of the left and right spokes so that the robot can work stably on the stairs.

B. Ideal Dynamic Phase Difference

According to our assumption, the front and the rear wheels are expected to follow an identical optimal trajectory, resulting in a consistent and periodically varying phase difference. We conduct numerical simulations using MATLAB to capture the dynamic phase difference between wheels. Fig. 5 shows the dynamic phase differences over a single period while climbing a stair with dimensions of $300 \times 160mm$.

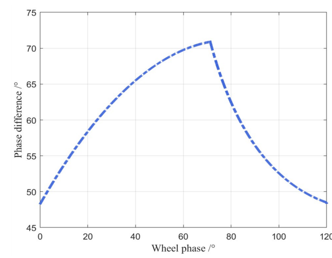

Fig. 5. Dynamic phase difference for smoothest stair climbing.

C. Motion Control in Simulation Environment and Field Test

The API within Webots simulation environment streamlines the control process, ensuring precise motor control. We set a specified speed for the front wheels and obtain the dynamic phase difference aiming to record the dynamic speed sequence for the rear wheels. This approach ensures a seamless and periodic stair-climbing motion.

We suppose to use the dynamic phase difference driving strategy to attain stable climbing performance for SWhegPro3 during field testing. However, during the preliminary experiment, we obtain unstable climbing results, which can be attributed to the intricate and variable nature of the actual operating environment. Furthermore, the M3508 motor can't precisely control its position, leading to uncontrollable errors.

Subsequently, we attempt a straightforward speed loop control approach and are surprised by its effectiveness. This approach enabled SWhegPro3 to climb stairs seamlessly. The successful outcome can be attributed to the interaction between the front and rear wheels, resulting in a balancing effect.

V. Work Scenario Definition: Stairs

Stairs are designed for human to walk with legs, but for robots specifically intend for stair climbing, the most considerable parameter is the steepness of the stairs. This is quantified by the physical quantity S, representing the slope of the stairs, and is defined as follows:

$$S = arctan(L/H) \quad (1)$$

Where S is measured by degrees, with an increase in S indicating steeper stairs. L represents the length of the stairs, while H corresponds to the height of the stairs. These two parameters are depicted in Fig. 2(a).

According to China's standard for stairs in civil buildings, the common size of stairs is divided into three grades, the size of which are large ($L = 300mm$, $H = 165mm$, $S = 28.81°$), medium ($L = 270mm$, $H = 150mm$, $S = 29.05°$), small ($L = 240mm$, $H = 135mm$, $S = 29.35°$), whose S value are all around $29°$.

Apart from the officially standard dimensions, there's a set of special sizes of stairs in various building types. We categorize stairs into the following three types:

- A-type stair: $240mm < L < 300mm$, $135mm < H < 165mm$, and $24.22° < S < 34.51°$.
- B-type stair: $300mm < L < 450mm$, $135mm < H < 165mm$, and $16.69° < S < 28.81°$.
- C-type stair: $240mm < L < 300mm$, $80mm < H < 135mm$, and $14.03° < S < 27.02°$.

On this basis, we design experiments to test the climbing performance of robots on different types of stairs. We can find that all the standard stairs are A-type stairs, thus A-type stairs are the most common types in daily life, their performance will be verified through both simulations and field tests. B-type and C-type stairs, while prevalent in reality, will be first assessed in the Webots simulation environment due to limitations of the parameters during the design phase.

VI. Field Experiments and Simulation

A. Stair Climbing Performance in Legged Mode

Consider the climbing condition of the robot on parallel stairs, its primary fluctuations occur along the orientation-y. As a result, we assess climbing stability by monitoring the pitch angle at the robot's geometric center. For this purpose, we put the IMU module at the geometric center of the robot during both simulation and field testing. The IMU module records and outputs pitch angle data in radians at $50Hz$.

After we definite the work scenario, stairs are categorized into three types: A, B, and C. We focus on identifying stairs that are commonly encountered in daily life.

Table I outlines the selection criteria and size details of the stairs that we are going to use.

TABLE I
Selected stair cases

Type	Length(mm)	Height(mm)	Slope
A1	260	165	32.42
A2	300	150	26.57
B1	340	165	25.89
C1	295	130	23.78
C2	300	80	14.93

To capture the robot motion pattern, we record data from five cycles after the robot reaches a stable climbing state. During the analysis, we compute the average value across these cycles to find both the average deviation and ΔPitch, which represents the average difference between pitch angles at the peak and the trough.

Fig. 6 shows the test results of stairs A1 and A2. We put the pitch angle obtained by simulation and field test in the same figure to compare the performance.

Referring to Table I, the slope value of staircase A1 is $32.42°$. During simulation, the average pitch angle during climbing stair A1 is $31.65°$, which deviates by $0.77°$ from the slope angle, the average maximum difference $\Delta\text{Pitch}^{Sim}_{A1} = 6.41°(19.77\%)$. In the field test, the average pitch angle while climbing stair A1 is $32.34°$, exhibiting a discrepancy of $0.08°$ from the slope angle, the average maximum difference $\Delta\text{Pitch}^{Field}_{A1} = 4.98°(15.36\%)$.

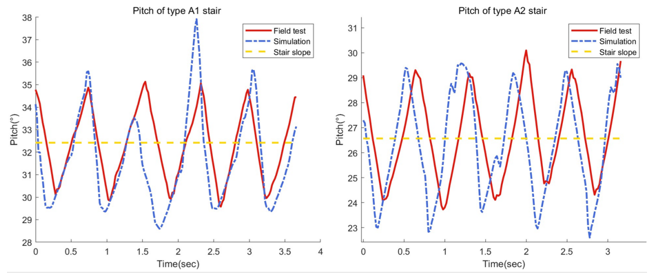

(a) (b)

Fig. 6. The pitch angle of SWhegPro3 robot over type-A stairs. (a)Stair A1. (b)Stair A2.

Referring to Table I, the slope value of staircase A2 is $26.57°$. During simulation, the average pitch angle during climbing stair A1 is $26.35°$, which deviates by $0.22°$ from the slope angle. This leads to an average maximum difference of $\Delta\text{Pitch}^{Sim}_{A2} = 6.39°$ (24.25%). In the field test, the average pitch angle observed while climbing staircase A1 is $26.65°$, resulting in a difference of $0.08°$ from the slope angle. This yields an average maximum difference of $\Delta\text{Pitch}^{Field}_{A2} = 5.28°$ (19.87%).

The data indicates that during the climbing process, the ΔPitch values for SWhegPro3 are consistently around $5°$, and the gap between the average pitch and the slope is little. Based on these observations, we can confidently conclude that the climbing performance of the robot on A-type stairs is outstanding.

We also observe an intriguing phenomenon: when not accounting for numerical lateral drift, ΔPitch values in the simulation are higher than in the field test. Furthermore, the average pitch angle in the field test has a smaller gap with the stair slope. This may be due to the timestamp error in the simulation environment, causing the front and rear wheels to fail to follow the dynamic phase difference.

When we test B-type stairs in the simulation environment, we find that the spoke length of 240mm is not enough: with each staircase climb, the contact point of the spoke with the next stair layer is positioned closer to the spoke's end. After climbing a certain number of stairs, the spokes will miss a step and collide with the flat surface below, leading to a pronounced drop in climbing stability. Meanwhile, the motors demand a greater torque to fulfill the climbing. The unstable climbing process is illustrated in Fig. 7(b).

Referring to Table I, the slope value of staircase A2 is $26.57°$. As shown in Fig. 7(a), the pitch angle exhibits an unmanageable upward trend, we deduce that the present design might not perform well when facing B-type stairs.

During the field test of the robot on C-type stairs, we observe the limitations of the curved-spoke design. As shown in Fig. 2(a), the stoppers easily miss the stairs, then the spokes obstructed by the stairs, resulting in the failure

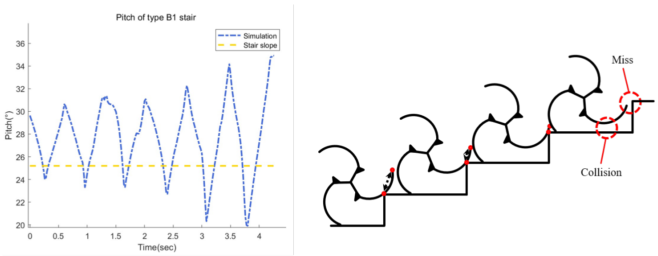

(a) (b)

Fig. 7. Principle of unstable climbing. (a)The pitch angle of SWhegPro3 over type-B stair. (b)Robot unstable climbing principle schematic.

climbing of the robot. As shown in Fig. 3(a), the stoppers are fixed to the center plate and cannot adjust their position. Consequently, we intend to control the extension length of the electric push rod, aiming to ensure the spokes contact with the stair plane, thereby preventing any circumstance of getting stuck.

B. Refining Spoke Control for Ascending Low-Height Stairs

Through the derivation of analytic geometry, we establish a mapping relationship between stair dimensions and the extension length of the electric push rods. Equations (2) to (11) are the derivation process.

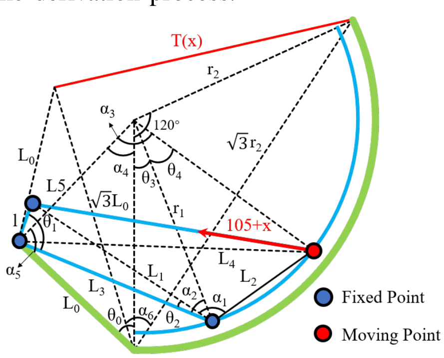

Fig. 8. Derivation of analytical geometry between electric push rod length and staircase dimensions.

In Fig. 8, the green lines depict the redesigned curve of the spoke, while the blue line represents the primary structural element of the physical object. Additional black dashed lines are auxiliary components use in the geometric operations. The red arrow indicates the length of the electric push rod x, and the solid red line corresponds to the dependent variable $T(x)$ that has been solved.

As the length of the electric push rod is constantly changing, some quantities are constant, among which: $\theta_0 = 50°$, $\theta_1 = 92.72°$, $\theta_2 = 9.86°$, $\theta_3 = 21.53°$, $\theta_4 = 34.05°$, $r_1 = 114mm$, $r_2 = 124mm$, $l = 20mm$, $L_1 = 116.67mm$, $L_2 = 66.76mm$, $L_3 = 114mm$, $L_{Arc} = 240mm$.

Following are the analytic geometry derivation formulas, all the unknowns are shown in Fig. 8.

$$\alpha_1 = \arccos(\frac{L_1^2 + L_2^2 - (105 + x)^2}{2L_1L_2}) \tag{2}$$

$$L_4 = \sqrt{L_2^2 + L_3^2 - \cos(\alpha_1 + \theta_2) * 2L_2L_3} \tag{3}$$

$$\alpha_2 = \alpha_1 + \theta_2 - \frac{(180° - \theta_4)}{2} \tag{4}$$

$$L_5 = \sqrt{r_1^2 + L_3^2 - \cos\alpha_2 * 2r_1L_3} \tag{5}$$

$$\alpha_3 = \arccos(\frac{L_5^2 + r_1^2 - L_4^2}{2L_5r_1}) \tag{6}$$

$$\alpha_4 = \alpha_3 - \theta_3 - \theta_4; \alpha_6 = 180° - \alpha_5 - \alpha_4 \tag{7}$$

$$L_0 = \sqrt{r_2^2 + L_5^2 - \cos\alpha_4 * 2r_2L_5} \tag{8}$$

$$\alpha_5 = \arccos(\frac{L_5^2 + L_0^2 - r_2^2}{2L_5L_0}) \tag{9}$$

$$T(x) = \sqrt{(\sqrt{3}L_0)^2 + (\sqrt{3}r_2)^2 - \cos\alpha_6 * 6L_0r_2} \tag{10}$$

$$T_{Aim} = \sqrt{H_s^2 + (L_s - L_{Arc})^2} \tag{11}$$

Among Equation 11, the H_s and L_s target height and depth of the stairs, respectively, T_{Aim} stands for the ideal value of T. Therefore, the x value which makes $T(x) = T_{Aim}$ is the length of the electric push rod.

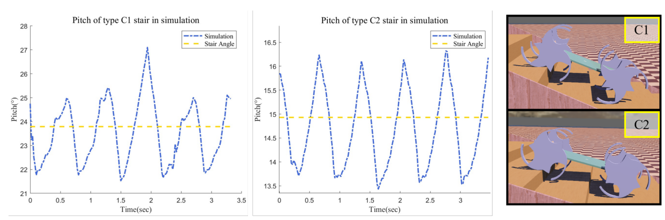

(a) (b) (c)

Fig. 9. Pitch angle of the SWhegPro3 over C-type stair in simulation. (a)Stair C1. (b)Stair C2. (c)Simplified SWhegPro3 in simulation environment.

To validate the accuracy of our mathematical model, we simulate the robot climbing in two C-shaped stairs. To lower the computational load, we recreate the corresponding simplified wheelsets model in SolidWorks, and then deploy it for experimentation in the Webots simulation environment. The simulation model is depicted in Fig. 9.

Referring to Table I, the slope value of staircase C1 is 23.78°, C2 is 14.93°. Fig. 9(a) and (b) portrays the test outcomes of the robot's engagement with stairs C1 and C2 in the simulation environment. While the average pitch angle slightly deviates from the slope of the stairs by $-0.26°$ and $-0.22°$, a marginally higher discrepancy compared to the result in stair A1 and A2 cases, the ΔPitch values reduce. Specifically, $\Delta\text{Pitch}_{C1}^{Sim} = 3.91°$ (16.43%), $\Delta\text{Pitch}_{C2}^{Sim} = 2.61°$ (17.48%).

These data indicate that: when compared with A-type stairs, the C-type stairs exhibit smaller ΔPitch values, suggesting that the robot's stair-climbing performance becomes smoother after adjusting the electric push rod length.

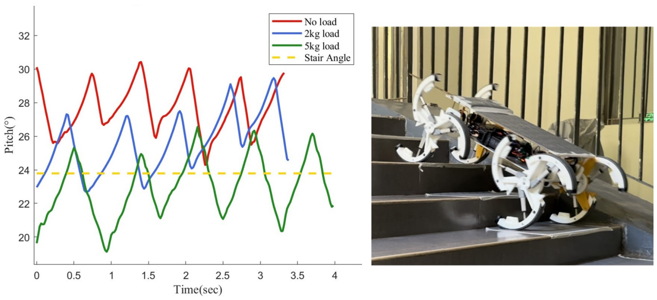

(a) (b)

Fig. 10. Different loads test in the field. The pitch angle (a) and the snapshot (b) of the SWhegPro3 robot during field experiments.

We observe substantial horizontal drift when the robot climbs on C1-type staircase without any load: The average pitch angle value measured 27.62°, surpassing the slope of the staircase 3.83° (16.09%). This discrepancy implies that an uneven torque output between the front and rear wheels may lead the robot to roll over. Consequently, we apply a load onto the front of the robot to shift its gravity center as far forward as possible. Fig. 10(a) illustrates the pitch angle variation when different weight loads are added.

When the external load is 2kg, the average pitch angle of the robot over C1-type stair is 25.61°, which is different from the slope 1.82°(7.65%). When the external load is 5 kg, the average pitch angle of the robot is 22.97°, which is different from the slope 0.82°(3.45%). It can be inferred that the risk of tipping is lower when the robot has a certain load on the forward.

C. Maximum load and speed test

We further conduct both maximum speed and maximum load tests. However, considering the potential tipping hazard while performing the maximum speed test on a steeper staircase, the maximum series tests are put on C1-type stair.

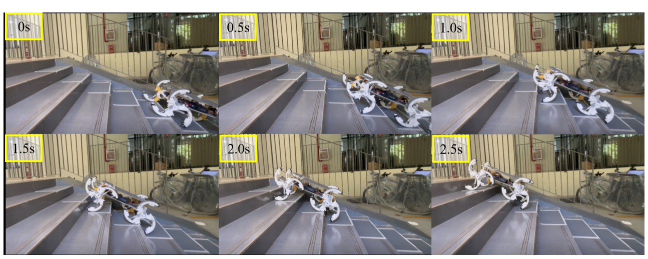

Fig. 11. The maximum climbing speed test of SWhegPro3.

During the maximum speed test, we measure a peak speed of approximately 1.8 steps per second, translating to a mere 2.8 seconds for climbing five stairs. When attempting even higher speeds, we encounter a pivotal constraint: higher target speed lead to excessive torque output, causing the robot to tip over or slip. Consequently, strategies such as redistributing the body's weight and enhancing the spokes' friction-generating capability are considered avenues to augment the robot's maximum climbing speed.

During the maximum load test, we realize a stable climbing with an external load of 7kg. Heavier external loads lead to low-speed climbing and exhibit slippery of the belt, which is unsafe.

VII. Conclusions & Future Work

This paper reports the system design and performance validation of a novel wheel-leg transformable robot. Compared with its predecessor, the new robot uses three-impeller design to significantly improve the overall stair-climbing performance. Moreover, instead of using push rod as a pure mode stitching actuator (binary operation: fully open and fully close), we can control its displacement for better adaptation to different-sized stairs in the new design. We also analyze the stair-climbing operation and derive a model to calculate the optimal configuration of the wheel-leg module and the corresponding displacement of the push rod. We conduct both simulation and field experiments to validate our proposed design and control strategy.

Future work includes using better driving motor alternatives (more powerful than the current M3508 motor), an online adjustment mechanism of the front and rear wheelbase for better stair negotiation performance, onboard 3D perception of stair geometry parameters to adjust the push rod displacement for autonomous operation.

Acknowledgments

This work was supported in part by the Guangdong Natural Science Fund-General Programme under grant no. 2021A1515012384. It was also supported by the Science, Technology and Innovation Commission of Shenzhen Municipality under grant no. ZDSYS20200811143601004, and the National Science Foundation of China(NSFC)#U1913603.

References

[1] W.-H. Chen, H.-S. Lin, Y.-M. Lin, and P.-C. Lin, "Turboquad: A novel leg–wheel transformable robot with smooth and fast behavioral transitions," *IEEE Transactions on Robotics*, vol. 33, no. 5, pp. 1025–1040, 2017.

[2] U. Saranli, "Rhex: A simple and highly mobile hexapod robot," *The International Journal of Robotics Research*, vol. 20, no. 7, pp. 616–631, 2001.

[3] E. Moore, D. Campbell, F. Grimminger, and M. Buehler, "Reliable stair climbing in the simple hexapod'rhex'," in *Proceedings 2002 IEEE International Conference on Robotics and Automation (Cat. No. 02CH37292)*, vol. 3, pp. 2222–2227, IEEE, 2002.

[4] D. Campbell and M. Buehler, "Stair descent in the simple hexapod'rhex'," in *2003 IEEE International Conference on Robotics and Automation (Cat. No. 03CH37422)*, vol. 1, pp. 1380–1385, IEEE, 2003.

[5] G. Quaglia, L. Bruzzone, R. Oderio, and R. P. Razzoli, "Epi. q mobile robots family," in *ASME International Mechanical Engineering Congress and Exposition*, vol. 54938, pp. 1165–1172, 2011.

[6] L. Bai, J. Guan, X. Chen, J. Hou, and W. Duan, "An optional passive/active transformable wheel-legged mobility concept for search and rescue robots," *Robotics and Autonomous Systems*, vol. 107, pp. 145–155, 2018.

[7] D. Choi, Y. Kim, S. Jung, J. Kim, and H. S. Kim, "A new mobile platform (rhymo) for smooth movement on rugged terrain," *IEEE/ASME Transactions on Mechatronics*, vol. 21, no. 3, pp. 1303–1314, 2016.

[8] C. Dai, X. Liu, J. Zhou, Z. Liu, Z. Zhu, and Z. Jia, "Swhegpro: A novel robust wheel-leg transformable robot," in *2022 IEEE International Conference on Robotics and Biomimetics (ROBIO)*, pp. 421–426, IEEE, 2022.

[9] Y. Kim, J. Kim, H. S. Kim, and T. Seo, "Curved-spoke tri-wheel mechanism for fast stair-climbing," *IEEE Access*, vol. 7, pp. 173766–173773, 2019.

[10] C. Zheng and K. Lee, "Wheeler: Wheel-leg reconfigurable mechanism with passive gears for mobile robot applications," in *2019 International Conference on Robotics and Automation (ICRA)*, pp. 9292–9298, IEEE, 2019.